Chaos, Solitons and Fractals 211 (2026) 118809

Contents lists available at ScienceDirect

Chaos, Solitons and Fractals

journal homepage: www.elsevier.com/locate/chaos

Heterogeneous collective criticality in cryptocurrency volatility: Scaling collapse, tail synchronization, and cascade amplification☆

Michael Zouari [a,*], Ilan Alon [a,b], Zeev Shtudiner [a]

[a] Department of Economics and Business Administration, Ariel University, Ariel, 40700, Israel
[b] Department of Strategic Management, Corvinus University of Budapest, Budapest, 1093, Hungary

ARTICLE INFO

Dataset link: Replication Package (Original data)

Keywords:
Critical boundary
Extreme event clustering
Cryptocurrency volatility
Long memory
Scaling collapse
Tail dependence
Self-organized criticality

ABSTRACT

This paper tests whether the volatility of Bitcoin (BTC), Ethereum (ETH), and Solana (SOL) is better characterized as a heterogeneous collective-critical regime than as asset-by-asset turbulence. Using daily and hourly data, with the daily S&P 500 cash index and the near-continuously-traded EUR/USD reference rate as contrast benchmarks, we extend the Bergmann–Oliveira critical-boundary framework from single-series classification to coupled volatility dynamics. Four results support the claim. First, Ethereum is robustly supercritical and Solana is supercritical under finite-sample validation, whereas Bitcoin is boundary-adjacent, with a point estimate below the boundary but a circular-block interval crossing $CR = 1$. Second, boundary distance and tail-clustering depth are distinct system-level coordinates: Solana has the largest boundary distance, while Bitcoin exhibits the slowest tail-dependence decay. Third, crypto clustering functions exhibit scaling collapse near a common exponent, $\beta \approx 0.31$, and pairwise and triadic co-exceedances remain above circular-shift, block-shuffle, and factor-residual null envelopes. Fourth, short-horizon volatility-of-volatility preserves cascade amplification, while long smoothing absorbs it; intraday boundary estimates are scale- and estimator-sensitive rather than fixed activation constants. The boundary configuration is not a conditional-heteroskedasticity artifact: heavy tails persist after GARCH/EGARCH/FIGARCH filtering, FIGARCH confirms genuine fractional integration, and a Gaussian-innovation GARCH cannot reproduce the observed supercriticality. The regime is further corroborated by marginal-matched surrogates that isolate the collective component. Conceptually, it recasts a single-series phase boundary as a diagnostic of synchronized collective instability. Practically, crypto tail risk should be monitored through boundary proximity, tail synchronization, and cascade propagation rather than marginal volatility alone.

1. Introduction

Financial markets exhibit regularities that are difficult to reconcile with models built on independence, thin tails, and smooth adjustment. Returns display little linear autocorrelation, yet their distributions are heavy-tailed; volatility clusters in time; and the autocorrelation of absolute returns decays slowly across horizons [1]. These markets are better understood as intensely fluctuating

☆ This article is part of a Special issue entitled: 'Tribute to Stefano Boccaletti' published in Chaos, Solitons and Fractals: the interdisciplinary journal of Nonlinear Science, and Nonequilibrium and Complex Phenomena.

* Corresponding author.
E-mail addresses: michael.zouari@msmail.ariel.ac.il (M. Zouari), ilan.alon@uni-corvinus.hu (I. Alon), zeevs@ariel.ac.il (Z. Shtudiner).

https://doi.org/10.1016/j.chaos.2026.118809
Received 28 April 2026; Received in revised form 15 June 2026; Accepted 7 July 2026
Available online 14 July 2026

ensembles of interacting heterogeneous agents: high-frequency records for the S&P 500 yield return distributions consistent with power-law tails whose exponent lies near 3 at short horizons, with crossover toward Gaussian behavior at longer horizons [2]. Price-change dependence vanishes quickly, whereas volatility displays persistent long-range correlations [3]. The same scaling extends beyond returns: exchange volume and trade frequency obey analogous power-law regularities [4]. Together, these stylized facts point to collective interaction rather than to independent shocks, and under crash conditions the fluctuation structure can approach the scale-invariant organization associated with critical phenomena [5]. Cryptocurrency markets, with their continuous trading and documented cross-asset spillovers, offer a particularly demanding laboratory for these questions.

The cryptocurrency literature documents these ingredients, but as separate strands. Bitcoin and other major cryptocurrencies exhibit time-varying persistence [6], asymmetric intraday multifractality [7], and dynamic multivariate dependence [8]; spillover studies show that crypto centrality is strong, time-varying, and not reducible to capitalization alone [9–11]. These results establish each ingredient separately, but they do not test whether these strands jointly define a phase-transition-like collective regime.

These ingredients have been analyzed in separate theoretical strands rather than within one phase-boundary framework. A first strand establishes that persistence resides in absolute and power transformations of returns rather than in raw returns, with the long-memory property peaking when the power is close to one [12]. A second strand shows persistence emerging from a multiscale cascade: a parsimonious heterogeneous volatility model can jointly reproduce long memory, heavy tails, and unifractal scaling, suggesting that persistence arises from interactions across horizons rather than from a single scale [13]. A third strand explains scale-free fluctuations through self-organized criticality: dynamical systems may evolve toward minimally stable configurations in which local perturbations propagate as avalanches and generate power-law temporal organization without external tuning [14].

What is still missing is an explicit bridge from these separate ingredients to a single framework governing the clustering of extremes. Bergmann & Oliveira [15] provide that bridge. For FARIMA (0, d, 0) processes with regularly varying innovations, they show that the joint action of memory persistence and tail heaviness is controlled by a critical threshold, $\alpha^* = 1/d$, which separates subcritical, critical, and supercritical regimes. In their high-frequency empirical application to S&P 500 futures, market states remain supercritical and drift toward the boundary during crisis periods. The unresolved question is whether this framework extends from a single financial series to the sampled BTC-ETH-SOL crypto core, in which contagion, synchronization, and multiscale amplification interact.

This paper addresses that gap by testing whether the sampled BTC-ETH-SOL volatility layer is better characterized as a heterogeneous collective-critical regime than as separate volatile assets. The empirical object is deliberately narrow: ETH and SOL are evaluated as the supercritical amplification core, while BTC is evaluated as a boundary-adjacent synchronization anchor. The claim is assessed conjunctively through boundary location with uncertainty, the separation of boundary distance from tail-clustering depth, scaling collapse, dependence-preserving co-exceedance, estimator-sensitive scale activation, and short-horizon volatility-of-volatility propagation.

The contribution is to shift the Bergmann–Oliveira critical boundary from a marginal classifier of one long-memory series to a system-level diagnostic of synchronized market instability, with heterogeneity treated as part of the regime concept rather than as deviation from it. The practical implication follows directly: risk monitoring should identify synchronized amplification states, where own-asset calibration and subcritical risk scaling are least reliable.

The remainder of the article follows this sequence. Section 2 defines heterogeneous collective criticality and derives three collective predictions. Section 3 presents the data, observables, and empirical design. Section 4 reports four layers of evidence: volatility-layer phase location, scaling collapse with estimator-sensitive scale activation, tail synchronization beyond dependence-preserving nulls, and short-horizon cascade propagation with risk-monitoring implications. Section 5 discusses the theoretical contribution, limitations, and higher-order extensions, and Section 6 concludes.

2. Critical-boundary framework for heterogeneous collective criticality

2.1. Temporal tail dependence and the critical boundary

The formal backbone of this study is the critical-boundary framework of Bergmann & Oliveira [15]. Rather than treating long memory and heavy tails as parallel stylized facts, they show that the two jointly determine the asymptotic organization of extremes through temporal tail dependence. The relevant quantity is the lag-k upper-tail dependence coefficient, $\lambda_U(k)$, defined as the limit, as the threshold grows without bound, of the conditional probability that an extreme exceedance at time t is followed by an exceedance of the same threshold at time t + k. For FARIMA (0, d, 0) processes with regularly varying innovations, the interaction between the memory parameter d and the tail index α is governed by a critical boundary at $\alpha^* = 1/d$.

This boundary yields three regimes. When $\alpha > \alpha^*$, the system is subcritical and extremes become asymptotically independent across time. When $\alpha = \alpha^*$, the system sits at the critical boundary and tail clustering obeys a logarithmically modified law. When $\alpha < \alpha^*$, the system is supercritical and temporal tail dependence decays as a power law, $\lambda_U(k) \sim k^{(d-1)\alpha}$, implying persistent clustering of extreme events rather than rapid decorrelation [15]. Because H = d + 1/2, the same boundary can be read as a joint phase diagram in the space of persistence and tail heaviness.

Empirically, the paper summarizes regime location by $CR_i = \alpha_i \cdot d_i$, where $CR_i < 1$ denotes supercriticality. Because the test is applied at the volatility layer, α_i and d_i are estimated on the same volatility-layer observable rather than on raw returns. The boundary is therefore a marginal phase-location device; the system-level contribution of this paper begins when that boundary is embedded in a coupled volatility system.

2.2. Volatility as the state variable

The critical-boundary framework is applied to volatility rather than signed returns because persistent dependence in financial markets is concentrated in volatility-layer observables [1,3]. Signed returns may be heavy-tailed, but their dependence decays quickly; absolute returns and realized volatility retain the long-range structure required by the framework [12]. The canonical state variable is therefore |r_t|, with realized-volatility analogues used for multiscale and cascade tests; raw returns are retained only as a state-variable check.

2.3. From single-series to collective criticality

Bergmann & Oliveira [15] formulate the problem at the level of a single long-memory series. That is the correct analytical starting point, but it is not yet a system-level description. Financial markets are coupled systems in which shocks propagate through overlapping positions, common liquidity conditions, and feedback trading, and are transmitted, amplified, or synchronized across assets. As established in the introduction, increasing interconnectedness can push financial systems across sharp thresholds [16], and the system-wide effect of a shock can exceed the initial perturbation substantially [17].

This system-level move requires a richer interaction language than simple pairwise correlation. Many complex systems cannot be adequately represented by dyadic links, because higher-order and group-level interactions change the dynamics in ways that pairwise reductions miss [18,19]. Multilayer systems can behave very differently from single-layer networks because multiple simultaneous channels of interaction reshape diffusion, spreading, and synchronization [20]. Once multiple assets are exposed to multilayer couplings, the relevant question is no longer whether each asset is individually close to criticality, but whether the market as a coupled ensemble exhibits collective criticality.

In this paper, collective criticality means that the market's extreme fluctuations are organized at the level of the interacting asset set, not at the level of individual series. Coupling can produce synchronized exceedances, shared regime shifts, and cross-asset reinforcement that together create a mode of instability invisible to single-series analysis. This extension moves the Bergmann & Oliveira framework from isolated criticality to systemic criticality.

2.3.1. Operational definition of heterogeneous collective criticality

To prevent the term collective criticality from functioning as a metaphor, the paper defines it as a heterogeneous system-level configuration. Let A denote the sampled crypto system, and let $A = C \cup B$, where C is the supercritical amplification core and B is the set of boundary-adjacent synchronization anchors. For each asset i, let $E_{i,t}(q)$ denote the q-tail exceedance indicator computed after asset-specific standardization.

The system is said to exhibit heterogeneous collective criticality at horizon h and threshold q when four conditions jointly hold. First, at least one connected sub-core C lies robustly on the supercritical side of the Bergmann–Oliveira boundary, assessed by $CR_i < 1$, circular-block confidence intervals, and $P(CR_i < 1)$. Second, boundary-adjacent assets in B are not required to be robustly supercritical, but must remain close to the boundary and synchronize strongly with the supercritical core. Third, clustering functions must exhibit statistically significant scaling collapse relative to null envelopes. Fourth, pairwise and higher-order co-exceedances must exceed dependence-preserving null expectations, with short-horizon volatility-of-volatility preserving the cascade. This formulation defines heterogeneity as part of the regime concept, not as a deviation from it: the architecture of a robust amplification core coupled to a boundary-adjacent anchor is admitted ex ante, before any asset-specific evidence is examined.

For interpretation, the paper reports two distinct coordinates. The signed distance-to-boundary statistic $\Delta_i = 1 - CR_i$ records whether an asset lies below or above the Bergmann–Oliveira boundary and how far it is from that boundary. It is a regime-location coordinate, not a direct measure of clustering intensity. The temporal tail-dependence decay exponent $\delta_i = (d_i - 1)\alpha_i$ records the asymptotic decay rate of $\lambda_U(k)$ once the series is in the supercritical regime. Less negative δ_i implies slower decay and therefore deeper temporal clustering. Reporting both Δ_i and δ_i keeps the regime classification distinct from the strength of the clustering process.

2.3.2. Probabilistic boundary inference

The boundary is interpreted probabilistically rather than deterministically. All classifications are reported with circular-block intervals and $P(CR_i < 1)$, and all cross-asset exceedances are defined by asset-specific quantiles, so that synchronization is evaluated in standardized tail space and not in raw volatility units. The full set of stationarity, fractional-persistence, regular-variation, and estimation assumptions is documented in Methods (Section 3) and Supplementary Appendix A.

2.3.3. Anchor-amplifier architecture and synchronization intensity κ

The definition admits a structural specialization. In heterogeneous coupled markets, the asset that coordinates the system need not be the asset that lies deepest in the supercritical region. Collective instability can instead be organized by an anchor-amplifier architecture. A benchmark asset may remain boundary-adjacent when volatility-layer memory and tail heaviness jointly place αd close to one, while still retaining systemic coordination power through tight synchronization with the rest of the block. Platform assets with weaker volatility-layer memory sit farther below the critical threshold $\alpha^* = \frac{1}{d}$ and can therefore occupy the interior of the supercritical region.

Operationalizing this picture requires a third coordinate beyond the boundary distance Δ_i and the decay exponent δ_i. Let $R_{ij}(q)$ denote the observed q-tail co-exceedance ratio between assets i and j, and let $R_{ij}^{null}(q)$ denote the 95th percentile of a dependence-preserving circular-shift null envelope. The null-adjusted synchronization intensity of asset i with the rest of the crypto block A is given by

$$\kappa_i(q) = \frac{1}{|A|-1} \sum_{j \neq i, j \in A} \frac{R_{ij}(q)}{R_{ij}^{\text{null}}(q)}$$

A boundary anchor has small or interval-crossing Δ_i, relatively slow δ_i, and high κ_i. A supercritical amplifier has robustly positive Δ_i and high synchronization intensity. Section 4.3 applies this classification to the BTC-ETH-SOL triad. κ_i is treated as a system-level synchronization coordinate and is reported with circular-block uncertainty. Its stability is evaluated across tail thresholds $q \in \{0.90, 0.95, 0.99\}$ and across circular-shift, block-shuffle, and factor-residual nulls. The role classification is retained only when the synchronization ranking and qualitative anchor/amplifier assignment are stable across these specifications.

2.4. Observable signatures of collective criticality

Once the market is framed as a coupled critical system, the theory yields observable macroscopic signatures. The first signature is scale invariance. Systems near minimally stable states generate scale-free fluctuations and avalanche-like propagation [14], and financial crash dynamics can approach a critical regime in which non-Gaussian fluctuations become scale-invariant and distributions collapse across horizons [5]. If cryptocurrency markets display an analogous organization, clustering functions measured at different time scales should not remain idiosyncratic; after proper normalization, they should collapse toward a common functional form.

The second signature is synchronization. In interacting systems constrained by a network topology, coherence depends on both the architecture of connections and the coupling among elements [21]. In markets, this implies that extremes should not simply occur more often; they should align more strongly across assets when collective instability intensifies. Interacting-agent dynamics can generate volatility clustering, intermittent bursts, and power-law tails through collective rather than isolated mechanisms [22].

The third signature is hierarchical propagation. In a critical system, instability should not remain confined to a single layer of fluctuations; it should cascade from returns to volatility and from volatility to higher-order fluctuation measures. After a market crash, threshold exceedances decay according to a power law analogous to the Omori law in seismology, implying that extreme activity relaxes without a characteristic time scale [23]. The critical-boundary framework therefore predicts not merely higher volatility, but a specific multiscale pattern: scaling collapse across horizons, cross-asset synchronization of extremes, and hierarchical self-amplification across fluctuation layers. These are the observable signatures that distinguish a collective-criticality interpretation from standard short-memory risk models.

Scale activation is treated as a crossover diagnostic. A coupled critical system need not show the same effective regime at every sampling frequency: short horizons may contain microstructure noise and local liquidity effects that obscure the persistence-tail interaction. The critical activation horizon $T_i^{\dagger}$ therefore identifies the shortest aggregation scale at which the boundary condition becomes visible, but exact activation horizons are interpreted diagnostically rather than as structural constants.

2.5. Collective predictions

P1. Heterogeneous boundary organization

The BTC-ETH-SOL volatility layer should contain a supercritical amplification core coupled to a boundary-adjacent synchronization anchor, rather than uniform marginal supercriticality across all assets and horizons.

P2. Multiscale collective synchronization

Clustering functions should collapse after rescaling, and extreme events should synchronize across assets beyond dependence-preserving null expectations.

P3. Scale-activated cascade propagation

Critical organization should propagate horizontally across the crypto block and vertically into short-horizon volatility-of-volatility, while long smoothing should absorb the cascade and reveal the scale-activated nature of the regime.

These predictions are conjunctive. Boundary classification alone could reflect marginal heavy-tailed volatility; scaling collapse rules out purely horizon-specific clustering; dependence-preserving nulls rule out coincidence or a single common factor; and short-horizon volatility-of-volatility tests vertical propagation. The regime is inferred only when phase location, scaling geometry, synchronization, scale activation, and cascade propagation align. While this synthesis combines several theoretical traditions rather than deriving from a single generative model, the conjunctive structure is intentionally falsifiable: any one signature could fail empirically and weaken the collective-criticality reading.

3. Data, observables, and empirical design

3.1. Data universe, benchmark, and sampling structure

The empirical design is built around a primary crypto panel composed of Bitcoin (BTC), Ethereum (ETH), and Solana (SOL), observed at both daily and hourly frequency. BTC is available from August 2017, ETH from January 2018, and SOL from August 2020 through 5 April 2026. The traditional-market benchmark is the S&P 500, observed daily from January 2006 through 2 April 2026. As a second contrast benchmark, we add the ECB daily euro–dollar reference rate, drawn from the near-continuously traded FX market. Because it is observed at daily reference frequency, it is used as a daily contrast benchmark rather than as an intraday replication. Its values are reported alongside the S&P 500 in Tables 1 and 2a–2b, with window dependence detailed in Appendix J. BTC and ETH are the two longest and most institutionally central crypto series, and BTC has served as the benchmark asset in early long-memory studies of digital assets [6]. Connectedness studies further show that large cryptocurrencies form an interdependent market rather than a collection of isolated price processes, which makes a system-level design preferable to a single-asset case study [9].

The main tests use BTC, ETH, and SOL. These three assets satisfy two requirements that justify a focused, three-asset design rather than broader coverage. First, they span the cross-section of cryptocurrency markets along the key dimensions: BTC as the dominant institutional asset, ETH as the leading smart-contract platform, and SOL as a younger high-volatility growth asset. Second, they are the only three cryptocurrencies for which both long daily histories (3+ years) and deep hourly histories (ranging from roughly 49,500 to 75,500 observations) are simultaneously available, enabling the multi-scale realized-volatility analyses that the critical-boundary framework requires. The three-asset design therefore trades breadth for the depth the critical-boundary framework requires. All timestamps are standardized to UTC. Univariate estimation uses each asset's full available history, whereas cross-asset contagion tests are run on common overlapping samples only, because the paper studies both within-series criticality and between-series synchronization. Daily data are the canonical layer for regime classification; hourly data are used to construct realized volatility and to test multiscale stability, not to redefine the main criticality classification. Table 1 summarizes the sample architecture and main descriptive moments.

3.2. Construction of observables

The baseline price increment is the continuously compounded return,

$$r_{i,t} = ln\, P_{i,t} - ln\, P_{i,t-1}$$

computed at both daily and hourly frequency for asset i. Because the central theoretical object is not the signed price change but the volatility structure of the market, the design also constructs volatility-sensitive observables. First, daily realized volatility is obtained from hourly returns as

$$RV_{i,t} = \sqrt{\sum_{h=1}^{H_t} {r_{i,t,h}}^2}$$

following the quadratic-variation logic of Andersen et al. [24]. Second, volatility-of-volatility is defined as the absolute first difference of daily realized volatility,

$$VV_{i,t} = \left|RV_{i,t} - RV_{i,t-1}\right|$$

This short-horizon absolute first difference is used deliberately. The Bergmann–Oliveira framework predicts preservation of scale-invariant amplification across adjacent fluctuation layers; a long rolling standard deviation imposes a characteristic smoothing scale and can mechanically absorb fast cascade bursts. The 20-day rolling standard-deviation proxy is therefore retained as a sensitivity check rather than as the canonical cascade variable.

Extreme events are defined through asset-specific tail thresholds rather than common absolute cutoffs. For any observable $x_{i,t}$, the exceedance indicator is

Table 1
Sample architecture and descriptive moments.

Series	Freq.	Daily obs.	Hourly obs.	SD (%)	Skew.	Ex. Kurt.
BTC	D + H	3153	75,549	3.60	−0.96	15.51
ETH	D + H	3016	72,273	4.57	−0.94	12.60
SOL	D + H	2063	49,495	6.14	−0.21	7.87
S&P 500	D	5093	–	1.23	−0.47	12.86
EUR/USD	D	7025	–	0.58	0.05	3.27

Note: D = daily, H = hourly. SD = standard deviation of daily log-returns, in percent. Ex. Kurt. = excess kurtosis relative to a Gaussian distribution (positive values indicate fatter tails). Hourly observations are used to construct daily realized volatility and are not included in the moment calculations.

Table 2a
Regime classification and tail-dependence decay metrics.

Asset	d	α	α^*	CR	$\Delta = 1 - \text{CR}$	$\delta = (d-1)\alpha$	Regime wording
BTC	0.306	2.955	3.266	0.905	0.095	−2.05	Boundary-adjacent supercritical
ETH	0.174	3.129	5.746	0.545	0.455	−2.58	Robust supercritical
SOL	0.109	3.029	9.212	0.329	0.671	−2.70	Supercritical (validated)
S&P 500	0.499	2.752	2.004	1.374	−0.374	−1.38	Daily benchmark subcritical
EUR/USD	0.376	3.904	2.659	1.469	−0.469	−2.44	FX benchmark subcritical

Note: d = long-memory parameter, estimated by DFA on $|r|$. α = tail index, median of six estimators. $\alpha^* = 1/d$ defines the critical boundary. CR = $\alpha \cdot d$, and $\Delta = 1 - \text{CR}$ is the signed distance from the boundary. $\delta = (d-1)\alpha$ is the Bergmann–Oliveira tail-dependence decay exponent in the supercritical regime; less negative values imply slower asymptotic decay of temporal tail dependence. Thus Δ and δ answer different questions: location relative to the boundary versus depth of temporal clustering.

Table 2b
Circular contiguous-block uncertainty for the criticality ratio.

Asset	CR point	95% CR interval	P(CR < 1)	Classification
BTC	0.905	[0.578, 1.176]	0.612	Boundary-adjacent
ETH	0.545	[0.470, 0.840]	1.00	Robust supercritical
SOL	0.329	[0.315, 0.795]	1.00	Supercritical (validated)
S&P 500	1.374	[1.034, 1.492]	0.008	Robust subcritical
EUR/USD	1.469	[1.214, 1.520]	0.000	Robust subcritical

Note: Intervals are percentile intervals from B = 1000 circular contiguous-block subsamples covering 80% of each series. The procedure is designed to preserve long-range volatility organization better than independent resampling. BTC is therefore reported as boundary-adjacent rather than deeply supercritical.

$$E_{i,t}(q) = 1\{|x_{i,t}| > Q_i(q)\}$$

where $Q_i(q)$ is the q-quantile of $|x_{i,t}|$. The baseline threshold is q = 0.95, while q = 0.90 and q = 0.99 are used in sensitivity checks. Volatility levels differ sharply across BTC, ETH, SOL, and the equity benchmark, so the empirical question is whether each market clusters its own extremes beyond what independence would imply [1]. For cross-asset analyses, exceedances are always defined relative to each asset's own distribution before synchronization and contagion are evaluated.

A complete dictionary of observables, parameters, and derived metrics is provided in Supplementary Table S1.

3.3. Estimation of memory and tails

Persistence is estimated canonically by DFA on $|r_t|$, with $d = H - 0.5$. GPH, Whittle-type, and wavelet estimates are retained as sensitivity checks in Supplementary Appendix A because persistence in crypto markets is scale-dependent and finite-sample sensitive [6,7].

Tail heaviness is summarized by α via a six-estimator consensus (adaptive Hill, double-bootstrap Hill, DEH bias-corrected, kernel, QQ, max-to-sum). Hill alone is sensitive to top-order-statistic choice [25], so the canonical α is the median of the six. Full estimator dispersion and threshold sensitivity are reported in Supplementary Appendix A.

3.4. Criticality metrics and multiscale diagnostics

Once d and α are estimated, the critical boundary is defined exactly as in Bergmann & Oliveira [15]:

$$\alpha_i^* = \frac{1}{d_i}$$

The paper's main classification statistic is the criticality ratio,

$$CR_i = \frac{\alpha_i}{\alpha_i^*} = \alpha_i d_i$$

$CR_i < 1$ denotes a supercritical regime, $CR_i = 1$ the critical boundary, and $CR_i > 1$ a subcritical regime. The manuscript uses one canonical specification throughout: d from DFA on $|r_{i,t}|$, α from the six-estimator median, and $CR = \alpha d$. When the analysis moves to realized volatility or vol-of-vol, the same estimator logic is applied layer by layer.

For any exceedance process E_t, the normalized clustering function is

$$\lambda(k) = \frac{P(E_{t+k} = 1 \mid E_t = 1)}{P(E_t = 1)}$$

Under supercriticality, $\lambda(k)$ decays as a power law [15], and critical financial regimes display scale invariance and data collapse after suitable rescaling [5]. The paper evaluates multiscale clustering in two steps. First, it estimates $\lambda(k)$ across multiple aggregation horizons. Second, it searches for a collapse exponent β that minimizes cross-horizon dispersion after rescaling, and compares the collapse quality to an unscaled benchmark and to permutation-based null envelopes. Extremal clustering is summarized further by the extremal index θ, estimated with the intervals estimator as the baseline and with runs and blocks estimators as sensitivity checks. A small θ indicates stronger temporal bunching of extremes, while a larger θ indicates more isolated exceedances. This combination of CR, $\lambda(k)$, and θ moves the analysis from parameter space to observable market organization.

3.4.1. Bootstrap inference for the criticality ratio

Because $CR_i = \alpha_i d_i$ combines two estimated quantities, point estimates alone are not sufficient for regime classification. The final inference uses $B = 1000$ circular contiguous-block subsamples, which preserve the chronological organization of long-memory volatility better than independent resampling. In each draw, a contiguous circular block covering 80% of the series is selected, d_i, α_i, and CR_i are re-estimated using the baseline pipeline, and the empirical CR_i distribution provides percentile intervals and $P(CR_i < 1)$. BTC is treated as boundary-adjacent because its interval crosses $CR = 1$; ETH is interpreted as robustly supercritical, and SOL as finite-sample-validated supercritical, because their intervals remain below the boundary.

These quantities (the CR point estimate, the $B = 1000$ circular contiguous-block interval, $P(CR_i < 1)$, Δ_i, δ_i, and regime wording) are reported in Tables 2a–2b. Complete subsampling specifications, null-model definitions, and computational settings are documented in Supplementary Appendix E.

3.5. Contagion, connectedness, and predictive design

Collective criticality is not only a univariate property. It should also appear as synchronized exceedances and lagged cross-asset amplification. For this reason, the paper extends the univariate clustering statistic to the cross-asset case via $\lambda_{ij}(k)$ (Supplementary Table S1), which captures whether an extreme in asset i raises the probability of a later extreme in asset j, normalized by j's unconditional extreme frequency. Contemporaneous co-exceedance ratios compare observed joint extremes to the independence benchmark $P(E_i = 1) \cdot P(E_j = 1)$. These measures translate the connectedness literature, which has shown that spillovers among cryptocurrencies are sizable and unevenly distributed [9–11], into an extreme-event language aligned with the paper's phase-transition framing.

A compact predictive block evaluates whether collective-criticality diagnostics carry forward information after amplification states. The main signal is $VR_{i,t}$, defined as short-run realized volatility relative to a trailing 30-day benchmark. Detailed ROC/AUC, conditional-coverage, and Diebold-Mariano [26] diagnostics are reported in Supplementary Appendix F; the main text uses them only to interpret the risk-monitoring implications of the collective regime.

3.5.1. Dependence-preserving nulls for collective synchronization

The independence benchmark is retained for interpretability but is no longer sufficient for the collective claim. The revised cross-asset design evaluates co-exceedances against dependence-preserving nulls. The circular-shift null randomly rotates each asset's exceedance sequence, preserving event counts and serial clustering while destroying cross-asset timing. The block-shuffle null preserves local burstiness through fixed-length (20-day) block resampling. A factor-residual null removes a common crypto market mode and tests whether residual extremes still synchronize beyond shared exposure. Pairwise co-exceedances are interpreted as collective only when they exceed the 95th percentile of the circular-shift null and remain directionally stable under at least one additional null.

The factor-residual null is constructed on standardized BTC-ETH-SOL daily log-absolute returns. The first principal component is estimated on the common sample, each series is residualized on that component, and residual exceedances are redefined using asset-specific quantiles. The test asks whether a single common crypto volatility mode exhausts synchronization; the construction is described here, and related null-robustness evidence is reported in Supplementary Table S3.

Because the empirical design includes multiple thresholds, nulls, and horizons, the paper separates confirmatory tests from sensitivity checks. The confirmatory synchronization tests are the $q = 0.95$ pairwise and triadic co-exceedance tests under circular-shift, block-shuffle, and factor-residual nulls. Sensitivity analyses at $q = 0.90$ and $q = 0.99$, alternative estimators, and additional horizons are reported as robustness exercises rather than as independent confirmatory tests. For the confirmatory p-values, both Holm family-wise error adjustment and Benjamini-Hochberg FDR adjustment are reported in Supplementary Table S5.

4. Findings

The findings proceed from marginal phase location to system-level organization: volatility-layer criticality, scaling collapse, tail synchronization, and vertical cascade. The collective claim is accepted only where these layers align.

4.1. Long memory resides in volatility, not returns

Across raw daily returns, the fractional-memory component remains close to zero for all assets. Volatility transformations sharply increase persistence: under the canonical DFA pipeline on $|r_t|$, $d = 0.306$ for BTC, 0.174 for ETH, 0.109 for SOL, and 0.499 for the S&P 500. Where hourly data are available, realized-volatility analogues are analyzed as a separate volatility layer. They confirm that persistence is concentrated in second-moment observables, but, as shown in Section 4.4, the realized-volatility CR itself is not uniformly supercritical; this distinction motivates the adjacent volatility-of-volatility cascade test. The persistent component is therefore a second-moment property rather than a signed-return property.

The canonical regime classification is obtained by combining the volatility-layer Hurst estimate with the six-estimator consensus tail index. That classification splits the crypto block from the traditional benchmark, but the split must be interpreted with two coordinates rather than one. BTC, ETH, and SOL all have $CR = \alpha d$ below one, with point estimates of 0.905, 0.545, and 0.329, respectively. The daily S&P 500 cash-index benchmark lies above the boundary with $CR = 1.374$. In terms of boundary location, BTC is closest to the boundary, ETH is farther inside the supercritical region, and SOL has the largest positive Δ. However, Δ is not a direct measure of temporal clustering depth.

The reason is that the Bergmann–Oliveira asymptotic decay rate is governed by $\delta_i = (d_i - 1)\alpha_i$, not by Δ_i alone. For the crypto assets, δ equals −2.05 for BTC, −2.58 for ETH, and −2.70 for SOL. Less negative values imply slower temporal tail-dependence decay. BTC is therefore boundary-adjacent in the phase diagram but exhibits the slowest asymptotic decay among the three crypto assets, whereas SOL is farthest from the boundary but has faster asymptotic decay. The final B = 1000 circular-block intervals sharpen the interpretation: ETH remains robustly supercritical and SOL finite-sample-validated supercritical, while BTC remains a near-boundary supercritical point estimate with non-negligible classification uncertainty (Tables 2a–2b).

The main implication of Tables 2a–2b is that collective criticality should not be equated with homogeneous marginal supercriticality. BTC is the most important case precisely because it is not deeply supercritical: its proximity to the boundary, slow tail-dependence decay, and later synchronization evidence make it a plausible coordination anchor rather than a marginal amplifier. ETH and SOL, by contrast, provide the supercritical interior of the crypto block. The phase diagram (Fig. 1) therefore already suggests a division of systemic roles: boundary anchoring in BTC and amplification in ETH/SOL.

Because SOL has the shortest history, the classification is also checked on a SOL-matched common window. Truncating BTC and ETH to SOL's calendar span and rerunning the boundary pipeline preserves the qualitative regime: BTC remains supercritical at the point estimate ($CR = 0.69$, $P(CR < 1) = 1.00$), and ETH remains supercritical ($CR = 0.64$, $P(CR < 1) = 1.00$). The full length-matched results are reported in Supplementary Table S2. The role classification is therefore not driven by the additional pre-2020 history available for BTC and ETH. Boundary classifications also remain stable across crisis and bear-market subperiods: ETH and SOL stay supercritical in every available subperiod, while BTC alternates between mildly supercritical and subcritical states across regimes (Appendix C; Supplementary Table S6).

SOL finite-sample reliability (Appendix I)

At SOL's sample size (N = 2063) the DFA estimator is essentially unbiased (bias −0.004 at d = 0.11; s.d. 0.043), so the wide CR interval reflects sampling variance rather than bias; the bias-corrected d is 0.112. CR remains below one across the entire plausible bias-corrected (d,α) box (maximum CR = 0.80), and a long-memory stochastic-volatility model calibrated to SOL gives P(CR < 1) = 1.00. We therefore describe SOL as supercritical at the point estimate, with classification uncertainty explicitly quantified rather than as deeply interior.

The S&P 500 should be read as a daily cash-index contrast benchmark rather than as an intraday replication of the Bergmann and Oliveira [15] futures application.

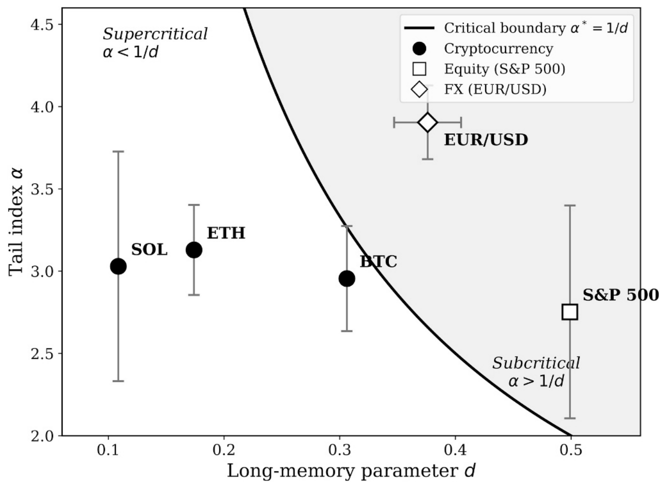

Fig. 1. Phase diagram of the volatility layer in the (d, α) plane.
Note: The solid curve is the critical boundary α* = 1/d, following Bergmann & Oliveira [15], which separates the supercritical regime (α < 1/d, shaded) from the subcritical regime (α > 1/d). Filled circles denote the three primary cryptocurrencies (BTC, ETH, SOL); the open square denotes the S&P 500 equity benchmark, and the open diamond the near-continuously-traded EUR/USD FX benchmark. Error bars show one standard error from the six-estimator tail-index consensus and from the DFA bootstrap on |r|. The crypto point estimates lie below the boundary, while the daily S&P 500 cash-index benchmark and the full-history EUR/USD benchmark lie above it. BTC is interpreted as boundary-adjacent because its CR interval crosses CR = 1; ETH is robustly supercritical and SOL finite-sample-validated supercritical under the reported subsampling exercise.

Robustness to volatility models (Appendix H)

The supercritical classification is not an artifact of conditional heteroskedasticity, but neither does it rest on residual marginal memory. GARCH/EGARCH/FIGARCH filtering absorbs most of the volatility-layer memory (residual $|z|$ memory $d \approx 0$), while the heavy tails survive (residual $\alpha \approx 2.8$–3.7). FIGARCH, the natural parametric competitor, returns a significantly positive fractional-integration parameter for crypto volatility (ETH $d = 0.39$, SOL $d = 0.23$), confirming genuine long-range dependence. A GARCH (1,1) calibrated to each series and simulated with Gaussian innovations yields CR $\approx$ 1.19–1.32 (subcritical) for every cryptocurrency. It cannot reproduce the observed crypto supercriticality (CR = 0.33–0.90) because its tails are too light, while it reproduces the S&P 500 subcritical value (sim 1.31 vs observed 1.37). The collective evidence therefore rests not on residual marginal supercriticality, but on the conjunction of heavy-tailed innovations, scaling geometry, and null-surviving cross-asset synchronization.

Second contrast benchmark, EUR/USD (Fig. 1, Tables 2a–2b, Appendix J)

Over its full 1999–2026 history the near-continuously-traded EUR/USD reference rate is robustly subcritical ($d = 0.376$, $\alpha = 3.90$, CR = 1.469, P(CR < 1) = 0.00), which reduces the concern that traditional-market subcriticality is driven only by equity's discrete, no-weekend trading. On the crypto-era window the EUR/USD estimate is boundary-adjacent (CR = 0.94) and on the SOL-matched window it is itself supercritical (CR = 0.61); near-continuous markets can therefore also cross the boundary in specific short regimes. The distinctiveness of the crypto block is therefore not marginal CR alone, but the conjunction of boundary behavior with unusually strong triadic synchronization and surrogate-resistant collective coupling.

4.2. Scale invariance and scaling collapse

For BTC, ETH, and SOL, clustering curves estimated at different aggregation horizons collapse toward a common functional form once rescaled by the asset-specific collapse exponent (Fig. 2). The reported point estimates are $\beta = 0.262$ for BTC, 0.298 for ETH, and 0.296 for SOL. The final B = 1000 bootstrap exercise shows that these estimates are statistically compatible with a shared value near 0.31 rather than literally identical: the 95% intervals are [0.190, 0.332] for BTC, [0.230, 0.362] for ETH, and [0.217, 0.380] for SOL. The quality of collapse improves relative to the unscaled benchmark. For BTC, the reproducible collapse loss Q falls from 0.037 to 0.005, an improvement factor of 7.5; for ETH, from 0.050 to 0.009 (×5.7); for SOL, from 0.052 to 0.011 (×4.7). Relative to permutation-based null envelopes, the observed collapses lie far outside randomized expectation ($z \gg 6$).

Scale collapse links the marginal boundary to collective organization. The result is not merely that each asset has clustered volatility; it is that clustering measured at different aggregation horizons can be mapped onto a common geometry. That common geometry makes the crypto block difficult to interpret as unrelated asset-specific bursts.

The multiscale boundary exercise refines the collective claim but also imposes an important qualification. Under the Hill-only intraday diagnostic, SOL crosses the boundary from 4 h aggregation, ETH from 8 h aggregation, and BTC remains near the boundary without a stable Hill-only activation. Under the six-estimator consensus pipeline, first-crossing horizons shift and become non-monotone across aggregation levels (Table 6; full ladders in Supplementary Table S4). Exact $T_i^{\dagger}$ values should therefore be interpreted diagnostically rather than as structural constants. The robust conclusion is one of scale-dependent heterogeneity: amplifier assets display repeated intraday crossings into the supercritical region, while BTC remains boundary-adjacent in the canonical daily classification and obtains systemic relevance through synchronization, slow tail-dependence decay, and boundary proximity.

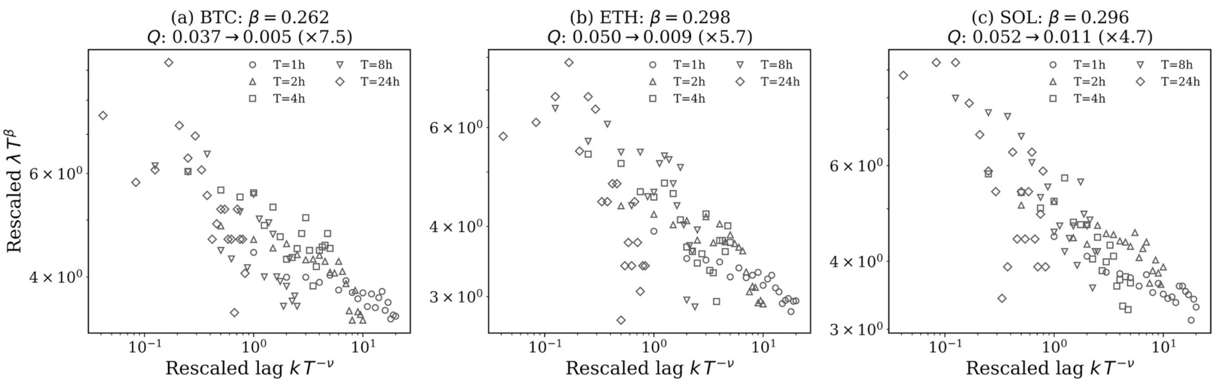

Fig. 2. Scaling collapse of the extremal clustering function in BTC, ETH, and SOL.
Note. Panels (a–c) show the rescaled extremal clustering functions for BTC, ETH, and SOL across five aggregation horizons (T = 1, 2, 4, 8, 24 h). After rescaling ($k \to k \cdot T^{-\nu}$, $\lambda \to \lambda \cdot T^{\beta}$), the curves collapse toward a common trend. Collapse exponents cluster near 0.31: $\beta = 0.262$ for BTC, $\beta = 0.298$ for ETH, and $\beta = 0.296$ for SOL; B = 1000 circular contiguous-block intervals overlap 0.31 for all three assets, supporting statistically compatible rather than identical scaling.

4.3. Collective organization during extremes

The connectedness literature already shows that cryptocurrency markets transmit return and volatility spillovers unevenly across assets [9–11]. The findings here sharpen that result by moving from average spillovers to synchronized tail events. In the extreme state, the market behaves as an organized collective rather than as a set of independent marginals.

The most direct evidence comes from co-exceedances. Table 3 ranks all pairs by their co-exceedance ratio relative to the independence benchmark and reports dependence-preserving null envelopes. The crypto-crypto block dominates: BTC-ETH co-exceed 11.24× above independence, with all crypto pairs above 6.4×. Cross-market alignment with the S&P 500 is weaker but still above both independence and dependence-preserving null envelopes, ranging from 3.09× to 4.22×. The crypto-crypto pairs are systematically stronger than the crypto-equity pairs, indicating that synchronization is concentrated within the crypto block rather than diffused uniformly across asset classes.

These null comparisons isolate the collective component of synchronization. For all crypto-crypto pairs, the observed co-exceedance ratio exceeds both the circular-shift and block-shuffle 95% envelopes with $p < 0.001$. The factor-residual test is even more conservative because it removes the first principal component of the crypto return block before redefining extremes. BTC-ETH falls from 11.24× to 5.90× after PC1 removal, showing that common market exposure explains part of the raw synchronization; however, 5.90× remains far above the residual circular-shift 95% envelope of 2.53×. BTC-SOL and ETH-SOL remain above their residual envelopes as well. Finally, the BTC-ETH-SOL triple-exceedance ratio equals 106.59× the independence expectation, while the circular-shift 95% envelope is only 5.61×. The synchronization result is therefore not reducible to a simple independence artifact or to one common factor.

Absolute counts and identification (Appendix K): the core of the collective claim

The BTC-ETH-SOL triple exceedance occurs on 19 of 1417 common days against an independence expectation of 0.18 (106.59×); pairwise joint-exceedance counts are 40 (BTC-ETH), 25 (ETH-SOL), 23 (BTC-SOL), 15/15 (BTC-/ETH-S&P) and 11 (SOL-S&P). To isolate what the framework uniquely captures, we simulate long-memory stochastic-volatility surrogates that match each asset's marginal d and α but contain no collective coupling: independent surrogates reproduce no triadic excess (≈1×) and a single common volatility factor reaches only ≈5× (the circular-shift envelope is 5.61×), whereas the observed 106.59× is more than an order of magnitude beyond both. Collective organization is thus the signature that marginal long-memory/heavy-tails and one common factor cannot generate; this, rather than marginal CR alone, is what the framework adds.

The PC1 residual test also reveals a useful asymmetry. The BTC-SOL residual co-exceedance ratio rises from 6.47× in the raw exceedance space to 11.24× after removal of the first crypto principal component, and ETH-SOL rises from 7.03× to 8.15×. This pattern is difficult to reconcile with a single-factor exhaustion interpretation, although residual ratios are interpreted cautiously because PC1 removal can alter covariance geometry in heavy-tailed data. Removing the dominant market mode does not eliminate crypto synchronization; for some pairs it unmasks pair-specific residual coupling that was partly hidden by the shared factor.

Additional directional diagnostics reinforce the same interpretation but are not central to the collective claim. Joint extreme moves are predominantly same-signed, crash synchronization exceeds rally synchronization, and lagged tail transmission is not reducible to market capitalization. These diagnostics are secondary and are reproduced in the replication package. The main point is that contemporaneous crypto synchronization survives dependence-preserving nulls and remains strongest precisely in the extreme state.

The κ coordinates complete the role classification (Table 4). BTC combines the smallest boundary distance and slowest decay exponent with high synchronization, making it a boundary-adjacent anchor. ETH and SOL supply the supercritical amplification core, with ETH also acting as a strong within-core coordinator. Because PC1-residual rankings are pair-sensitive, κ is used jointly with Δ, δ, boundary uncertainty, and activation behavior rather than as a standalone centrality parameter.

The synchronization evidence supplies the system-level step that the marginal boundary test cannot provide by itself. If the crypto assets were simply volatile in parallel, co-exceedances would disappear after preserving marginal clustering, shifting event calendars, shuffling burst blocks, or removing the first crypto principal component. They do not. The persistence of pairwise and triadic co-exceedances under these nulls indicates that the crypto core enters an extreme state jointly. This is the empirical basis for calling the regime collective rather than merely marginal.

All sixteen confirmatory synchronization p-values survive both Holm family-wise error adjustment (adjusted $p \leq 0.016$) and

Table 3
Joint-tail ratios and dependence-preserving null envelopes.

Pair	Observed/independence	Circular-shift 95% envelope	Block-shuffle 95% envelope	Null p-value
BTC-ETH	11.24×	1.97×	1.97×	<0.001
BTC-SOL	6.47×	2.25×	1.97×	<0.001
BTC-S&P	4.22×	1.97×	1.97×	<0.001
ETH-SOL	7.03×	1.97×	1.97×	<0.001
ETH-S&P	4.22×	1.97×	1.97×	<0.001
SOL-S&P	3.09×	2.25×	1.97×	<0.01

Note: The observed ratio is the number of joint extreme events divided by the independence expectation, with extremes defined as $|r|$ above each asset's own 95th percentile. The circular-shift and block-shuffle (20-day) envelopes ($B = 1000$ each) preserve marginal exceedance rates and serial clustering while breaking synchronized cross-asset timing. The reported p-value is the larger of the two dependence-preserving null p-values.

Table 4
Anchor-amplifier role classification within the crypto triad.

Asset	Δ	δ	κ ($q = 0.95$) circ/block/PC1	95% κ CI	κ rank stable	Role
BTC	+0.095	−2.05	4.77/4.60/2.90	[4.11, 5.86]	Yes (6/9 configs)	Boundary anchor
ETH	+0.455	−2.58	5.12/4.80/2.83	[4.23, 6.00]	Yes (6/9 configs)	Dual coordinator
SOL	+0.671	−2.70	3.45/3.60/3.31	[3.05, 5.55]	Yes (6/9 configs)	Fast amplifier

Note: $\Delta = 1 - CR$. $\delta = (d-1)\alpha$. $\kappa_i(q)$ is the mean of $R_{ij}(q)/R_{ij}^{null}(q)$ across other crypto assets in the block, where R_{ij}^{null} is the 95th percentile of the circular-shift, block-shuffle, or PC1-residual null envelope, depending on the column. The 95% κ CI is reported for the circular-shift null at $q = 0.95$ ($B = 1000$ circular contiguous-block bootstrap). κ rank stability is evaluated across nine configurations ($q \in \{0.90, 0.95, 0.99\} \times$ {circular-shift, block-shuffle, PC1-residual}).

Benjamini-Hochberg FDR adjustment (adjusted p $\leq$ 0.008). The collective synchronization claim is therefore not driven by multiple testing across thresholds, null specifications, or asset pairs. Detailed raw and adjusted *p*-values for each test family are reported in Supplementary Table S5.

4.4. Hierarchical volatility cascades

At the first volatility layer, proxied by $|r_t|$, all three cryptocurrencies remain supercritical. At the adjacent cascade layer, defined as short-horizon volatility-of-volatility, supercriticality also survives across the crypto block. The cascade is selective rather than mechanical: realized volatility and 20-day smoothed volatility-of-volatility do not remain uniformly supercritical. Long smoothing imposes a characteristic scale and absorbs the fast adjacent-layer amplification that the cascade test is designed to detect.

The stable hierarchical pattern is therefore three-level and short-horizon: weak or unstable persistence in returns, strong supercritical organization in volatility, and renewed supercritical organization in short-horizon volatility-of-volatility.

The three-layer criticality ratios are summarized in Table 5.

Long smoothing imposes a characteristic scale and is subcritical, whereas the short-horizon volatility-of-volatility re-enters the supercritical region: the scale-activated cascade.

This supports a scale-activated interpretation of cascade amplification.

4.5. Practical consequences of collective criticality

The practical implication of collective criticality is regime identification rather than universal forecasting superiority. After breaches, risk concentrates; after volatility surges, next-day extremes become more likely; and synchronized tail states weaken own-asset calibration. Detailed AUC, coverage, drawdown-scaling, and Christoffersen [27] diagnostics are reported in Supplementary Appendix F, with drawdown scaling in Supplementary Table S7a and cluster-adjusted practical-risk diagnostics in Supplementary Table S7b.

The boundary framework therefore does not replace GARCH, HAR, or other volatility models as universal forecasting devices. It identifies states in which local calibration logic becomes insufficient: synchronized tail states, post-breach amplification, and short-horizon cascade propagation. In those states, the relevant monitoring unit is the coupled crypto core rather than the isolated asset.

Appendix L provides an indicative horse-race between three next-day tail-risk specifications: own realized-volatility pressure alone, own-volatility plus cross-asset correlation, and a full collective-state specification including synchronization breadth/intensity and boundary proximity. The collective-state model does not deliver universal AUC dominance. Its value is concentrated where the framework is intended to operate: rare system-wide tail monitoring and probability calibration. For system-wide extremes, adding cross-asset correlation raises AUC from 0.812 to 0.825, while the full collective-state specification improves rare-class precision and calibration, increasing PR-AUC from 0.104 to 0.131 and reducing Brier loss from 0.0152 to 0.0149. Thus the practical contribution is not a replacement for volatility models, but a regime screen for synchronized tail states in which own-asset calibration becomes insufficient.

Table 5
Three-layer criticality ratios across volatility observables.

Layer	BTC	ETH	SOL	Regime
Returns $\lvert r\rvert$ (volatility proxy)	0.905	0.545	0.329	Supercritical
Realized volatility RV	1.54	1.28	1.07	Subcritical (absorbs cascade)
Short-horizon vol-of-vol $\lvert\Delta \mathrm{RV}\rvert$	0.54	0.33	0.36	Supercritical (cascade preserved)

Table 6
Diagnostic activation horizons under Hill-only and consensus tail estimation.

Asset	Hill-only $T_i^\dagger$	Consensus first crossing	Interpretation
BTC	Not activated/near-boundary	2 h, non-monotone	Boundary-adjacent anchor
ETH	8 h	1 h, non-monotone	Supercritical amplifier/dual coordinator
SOL	4 h	1 h	Fast amplifier

Note. The Hill-only column reports the shortest aggregation horizon at which $CR_i(T) < 1$ under the Hill [25] tail estimator alone. The consensus column reports the shortest crossing horizon under a six-estimator consensus α (Hill, double-bootstrap, DEH, kernel, QQ, max-to-sum). The two diagnostics disagree for every asset, so exact horizons are interpreted diagnostically rather than as structural constants; qualitative scale-dependent heterogeneity is the robust conclusion.

5. Discussion

5.1. Summary of evidence and collective interpretation

The main contribution is the change in empirical object. Bergmann and Oliveira's boundary classifies a single long-memory series; here it operates inside a coupled volatility block, where we ask whether phase location, scale geometry, synchronization, scale activation, and cascade propagation align. The evidence supports that system-level interpretation for the sampled BTC-ETH-SOL core.

The extension is heterogeneous rather than homogeneous. ETH and SOL define the supercritical amplification core, while BTC remains boundary-adjacent but coordinates the block through slow tail-dependence decay and null-surviving synchronization. This architecture was defined before role assignment and should be read as a bounded diagnosis, not as a universal claim about all crypto assets or all horizons.

5.2. Novelty relative to Bergmann–Oliveira

Bergmann & Oliveira [15] provide the decisive theoretical starting point by showing that the interaction between memory persistence and tail heaviness generates a critical boundary at $\alpha^* = 1/d$, separating subcritical, critical, and supercritical temporal organization of extremes. That contribution transforms heavy tails and persistence from parallel stylized facts into one phase-transition mechanism. The present paper retains that mechanism but changes both the state variable and the unit of analysis.

The state variable changes from signed returns to volatility-layer observables. As established in Section 2.2, absolute returns carry stronger and more persistent dependence than returns themselves [3,12], and volatility behaves as a heterogeneous cascade across horizons [13]. The paper's critical classification becomes meaningful only after this shift. In that sense, the paper does not transport the Bergmann–Oliveira method to another asset class; it redefines the state variable from raw price change to multiscale volatility organization.

The unit of analysis changes from a single long-memory series to a coupled crypto block. In the single-series setting, supercriticality implies persistent temporal clustering. Here, the same boundary logic coexists with strong cross-asset excess clustering (BTC-ETH-SOL triple co-exceedances at 107× independence), with 94% directional alignment in extreme windows, and with a further supercritical layer in short-horizon volatility-of-volatility where CR remains between 0.33 and 0.54 and tails are heavier than in the baseline volatility layer. The cryptocurrency market is therefore not just a set of supercritical marginals, but a supercritical collective regime.

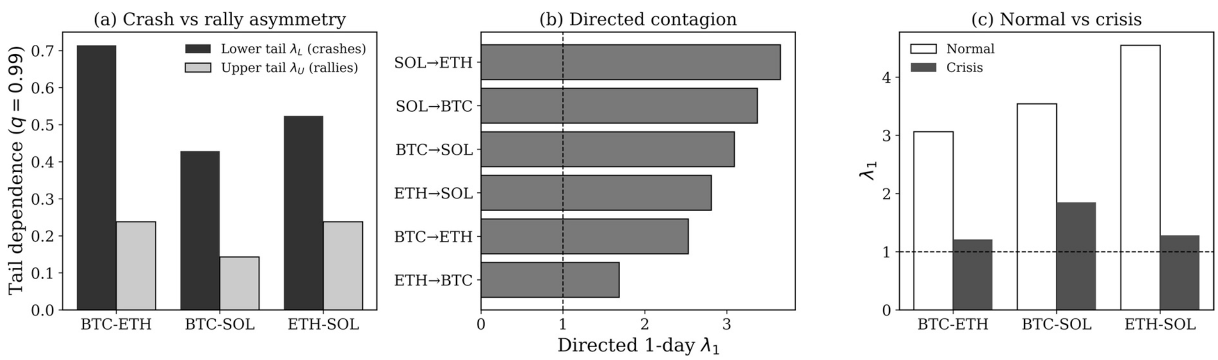

Fig. 3. Tail asymmetry and directed contagion structure in the BTC–ETH–SOL core.
Note: (a) Lower-tail (λ_L, black) vs upper-tail (λ_U, white) dependence at $q = 0.99$; crashes exceed rallies by 2.70× on average. (b) Directed one-day cross-clustering λ_1 for the six edges, sorted by magnitude; bar fill = source asset. SOL is the strongest transmitter, ETH the strongest receiver. (c) λ_1 in normal vs crisis windows for the three crypto pairs; lagged contagion weakens in crisis, with BTC → ETH approaching the no-excess line $\lambda_1 = 1$.

5.3. Structural supercriticality and the crypto collective mode

The connectedness literature has established that cryptocurrency spillovers are sizable and unevenly distributed [9–11], drawing on broader frameworks for synchronization in complex networks [21] and systemic risk in interconnected systems [16]. The present results extend that finding by showing that the relevant organization becomes sharper in the tail. In the extreme state, BTC-ETH-SOL triple co-exceedances exceed the independence benchmark by a factor of 107 ($p < 0.001$ against a circular-shift null; Table 3), crash dependence is 2.70 times stronger than rally dependence (Fig. 3a), and 94% of joint extreme moves share the same sign. Under extreme conditions, the market does not merely transmit shocks; it enters a synchronized regime that behaves less like a portfolio of distinct coins and more like a collectively organized state.

The structural character of this regime is equally important. Robustness checks across aggregation frequencies support a scale-activated interpretation, but the exact activation horizons are estimator-sensitive. The stable result is qualitative rather than metric-specific: ETH and SOL repeatedly enter the supercritical region across intraday aggregation designs, while BTC remains boundary-adjacent in the canonical daily classification and systemically relevant through synchronization. BTC is not a deep-supercritical case; it is a boundary-adjacent asset with slow asymptotic tail-dependence decay ($\delta = -2.05$; Table 2a). ETH and SOL are more decisively below the boundary, but SOL's larger boundary distance ($\Delta = 0.671$) does not translate into slower clustering than BTC: SOL's $\delta = -2.70$ indicates faster asymptotic decay than BTC's $\delta = -2.05$, so distance from the boundary and depth of temporal clustering are distinct system-level coordinates. Crypto instability is therefore better understood as the operating mode of a market whose volatility layer is close to cascade propagation and synchronized amplification, rather than as a simple ranking by CR magnitude.

These results admit an anchor-amplifier reading of the crypto market. Bitcoin functions as the boundary anchor: its strong volatility-layer memory ($d = 0.306$) combines with moderate tail heaviness ($\alpha = 2.955$) to place αd near the critical threshold, while its high null-adjusted synchronization intensity ($\kappa = 4.29$, computed on the four-asset envelope; cf. $\kappa = 4.77$ on the crypto-only null reported in Table 4, reconciled in the Supplementary Material) preserves systemic coordination power (Tables 2a, 4). Maturing informational efficiency and growing institutional presence plausibly contribute to this anchor role [28,29]. Ethereum and Solana function as the supercritical amplification core: their weaker volatility-layer memory ($d = 0.174$ and 0.109, respectively) raises the critical threshold $\alpha^* = 1/d$ into regions well above their observed α values, placing them farther inside the supercritical region. This position is consistent with smart-contract and protocol-dependency dynamics that generate episodic tail events without imposing long-range volatility persistence [30]. Recent high-frequency systemic-risk evidence supports this assignment, with Bitcoin and Ethereum as primary transmission sources and Solana among the most affected assets [31]. The collective claim therefore does not rest on homogeneous marginal supercriticality across every asset, but on a heterogeneous regime in which ETH is robustly supercritical while SOL is supercritical under finite-sample validation, and BTC acts as a boundary-adjacent coordinator with high persistence, moderate tails, and strong systemic synchronization. These mechanism-level interpretations are consistent with prior literature but are not directly identified by the present empirical design, which characterizes role differentiation rather than its causal substrate.

This interpretation is deliberately narrower than a universal claim about all cryptocurrencies. The evidence characterizes the sampled BTC-ETH-SOL core over the observed period. It does not imply that every crypto asset is supercritical, that every horizon is equally critical, or that BTC must be deeply below the boundary in every resample. The stronger and more informative claim is heterogeneous: an ETH/SOL amplification core is coupled to a BTC synchronization anchor, and the resulting regime becomes visible through scaling collapse, null-surviving co-exceedance, finite activation horizons, and short-horizon cascade propagation.

5.4. Mechanistic interpretation and risk-monitoring implications

Supplementary waiting-time and aftershock diagnostics are directionally consistent with a scale-free cascade interpretation (Appendix B; Appendix D), but the main claim does not rest on analogy to sandpiles or earthquakes. It rests on the alignment of phase-boundary location, scaling collapse, dependence-preserving synchronization, estimator-sensitive activation behavior, and short-horizon volatility-of-volatility propagation. The practical implication is conditional: existing volatility models remain useful, but their transportability depends on regime. When the BTC-ETH-SOL core enters synchronized amplification, regime-aware monitoring becomes more informative than continued reliance on own-asset calibration.

5.5. Future path toward higher-order crypto interactions

Future work should reconstruct the higher-order mechanisms behind this diagnosis by linking spot markets, derivatives, stablecoin liquidity, lending protocols, bridge activity, and layer-2 ecosystems in explicit multilayer or simplicial networks [18,20]. The present paper identifies the system-level regime; it does not yet map the mesoscopic structures that produce it.

6. Conclusion

This paper asked whether the coupled core of major cryptocurrencies (BTC, ETH, SOL) is better understood as separate volatile assets or as an interacting critical system. Viewed through the volatility layer, the answer is qualified but affirmative: ETH is robustly supercritical and SOL is finite-sample-validated supercritical, BTC is boundary-adjacent with slow asymptotic decay, and the crypto block displays dependence-preserving synchronization that cannot be reduced to independent marginals or to one common factor.

The paper contributes to complexity science in three ways. First, it extends the Bergmann–Oliveira critical-boundary framework from a single long-memory series to the level of collective market dynamics. Second, it separates boundary distance Δ from tail-dependence decay depth δ, resolving the apparent CR paradox that otherwise arises when SOL appears deeper by CR while BTC decays more slowly. Third, it demonstrates that instability propagates in two directions: horizontally across assets through scale-dependent intraday boundary behavior whose exact activation horizons are estimator-sensitive, and vertically across fluctuation layers instead of being absorbed at the first level of variation.

The practical implication is not simply that crypto risk is high. It is that the relevant risk state is collective. When the BTC-ETH-SOL core enters synchronized amplification, tail events become temporally clustered, cross-asset alignment strengthens, and short-horizon volatility-of-volatility preserves the cascade. Risk scaling, margining, and monitoring therefore become unreliable when they treat turbulence as an own-asset volatility problem and not as a coupled nonlinear regime. The external-validity target of these findings is the sampled BTC-ETH-SOL core, with the daily S&P 500 cash index as a contrast benchmark; generalization to other cryptocurrencies or to higher frequencies requires additional testing.

Two further qualifications follow from the new analyses. On crypto-matched short windows the EUR/USD estimate is boundary-adjacent (crypto-era, CR = 0.94) and even supercritical (SOL-matched window, CR = 0.61), so the benchmark contrast is anchored to full-history estimates. And the collective regime is identified relative to marginal and single-common-factor surrogates rather than to a fully structural generative model, which remains for future work.

CRediT authorship contribution statement

Michael Zouari: Writing – original draft, Visualization, Validation, Methodology, Investigation, Formal analysis, Data curation, Conceptualization. **Ilan Alon:** Writing – review & editing, Supervision. **Zeev Shtudiner:** Writing – review & editing, Supervision.

Declaration of competing interest

The authors declare that they have no known competing financial interests or personal relationships that could have appeared to influence the work reported in this paper.

Appendix A. Supplementary data

Supplementary data to this article can be found online at https://doi.org/10.1016/j.chaos.2026.118809.

Data availability

Data and code supporting this study are available in the OSF repository linked above; a permanent DOI will be activated upon acceptance.

Replication Package (Original data) (OSF)

References

[1] Cont R. Empirical properties of asset returns: stylized facts and statistical issues. Quant Finance 2001;1(2):223–36. https://doi.org/10.1080/713665670.
[2] Gopikrishnan P, Plerou V, Amaral LAN, Meyer M, Stanley HE. Scaling of the distribution of fluctuations of financial market indices. Phys Rev E 1999;60(5):5305–16. https://doi.org/10.1103/PhysRevE.60.5305.
[3] Liu Y, Gopikrishnan P, Cizeau P, Meyer M, Peng C-K, Stanley HE. Statistical properties of the volatility of price fluctuations. Phys Rev E 1999;60(2):1390–400. https://doi.org/10.1103/PhysRevE.60.1390.
[4] Gabaix X, Gopikrishnan P, Plerou V, Stanley HE. A theory of power-law distributions in financial market fluctuations. Nature 2003;423:267–70. https://doi.org/10.1038/nature01624.
[5] Kiyono K, Struzik ZR, Yamamoto Y. Criticality and phase transition in stock-price fluctuations. Phys Rev Lett 2006;96(6):068701. https://doi.org/10.1103/PhysRevLett.96.068701.
[6] Bariviera AF, Basgall MJ, Hasperué W, Naiouf M. Some stylized facts of the Bitcoin market. Physica A Stat Mech Appl 2017;484:82–90. https://doi.org/10.1016/j.physa.2017.04.159.
[7] Mensi W, Lee Y-J, Al-Yahyaee KH, Sensoy A, Yoon S-M. Intraday downward/upward multifractality and long memory in Bitcoin and Ethereum markets: an asymmetric multifractal detrended fluctuation analysis. Financ Res Lett 2019;31:19–25. https://doi.org/10.1016/j.frl.2019.03.029.
[8] Assaf A, Bhandari A, Charif H, Demir E. Multivariate long memory structure in the cryptocurrency market: the impact of COVID-19. Int Rev Financ Anal 2022;82:102132. https://doi.org/10.1016/j.irfa.2022.102132.
[9] Ji Q, Bouri E, Lau CKM, Roubaud D. Dynamic connectedness and integration in cryptocurrency markets. Int Rev Financ Anal 2019;63:257–72. https://doi.org/10.1016/j.irfa.2018.12.002.
[10] Koutmos D. Return and volatility spillovers among cryptocurrencies. Econ Lett 2018;173:122–7. https://doi.org/10.1016/j.econlet.2018.10.004.
[11] Sensoy A, Silva TC, Corbet S, Tabak BM. High-frequency return and volatility spillovers among cryptocurrencies. Appl Econ 2021. https://doi.org/10.1080/00036846.2021.1899119. Advance online publication.
[12] Ding Z, Granger CWJ, Engle RF. A long memory property of stock market returns and a new model. J Empir Financ 1993;1(1):83–106. https://doi.org/10.1016/0927-5398(93)90006-D.
[13] Corsi F. A simple approximate long-memory model of realized volatility. J Financ Economet 2009;7(2):174–96. https://doi.org/10.1093/jjfinec/nbp001.
[14] Bak P, Tang C, Wiesenfeld K. Self-organized criticality: an explanation of 1/f noise. Phys Rev Lett 1987;59(4):381–4. https://doi.org/10.1103/PhysRevLett.59.381.

[15] Bergmann DR, Oliveira MA. Extreme risk clustering in long-memory financial series. Chaos Solit Fractals 2026;202:117513. https://doi.org/10.1016/j.chaos.2025.117513.
[16] Haldane AG, May RM. Systemic risk in banking ecosystems. Nature 2011;469:351–5. https://doi.org/10.1038/nature09659.
[17] Bardoscia M, Barucca P, Battiston S, Caccioli F, Cimini G, Garlaschelli D, et al. The physics of financial networks. Nat Rev Phys 2021;3:490–507. https://doi.org/10.1038/s42254-021-00322-5.
[18] Battiston F, Cencetti G, Iacopini I, Latora V, Lucas M, Patania A, et al. Networks beyond pairwise interactions: structure and dynamics. Phys Rep 2020;874:1–92. https://doi.org/10.1016/j.physrep.2020.05.004.
[19] Boccaletti S, Latora V, Moreno Y, Chavez M, Hwang D-U. Complex networks: structure and dynamics. Phys Rep 2006;424:175–308. https://doi.org/10.1016/j.physrep.2005.10.009.
[20] Boccaletti S, Bianconi G, Criado R, del Genio CI, Gómez-Gardeñes J, Romance M, et al. The structure and dynamics of multilayer networks. Phys Rep 2014;544:1–122. https://doi.org/10.1016/j.physrep.2014.07.001.
[21] Arenas A, Díaz-Guilera A, Kurths J, Moreno Y, Zhou C. Synchronization in complex networks. Phys Rep 2008;469(3):93–153. https://doi.org/10.1016/j.physrep.2008.09.002.
[22] Krawiecki A, Hołyst JA, Helbing D. Volatility clustering and scaling for financial time series due to attractor bubbling. Phys Rev Lett 2002;89(15):158701. https://doi.org/10.1103/PhysRevLett.89.158701.
[23] Lillo F, Mantegna RN. Power-law relaxation in a complex system: Omori law after a financial market crash. Phys Rev E 2003;68(1):016119. https://doi.org/10.1103/PhysRevE.68.016119.
[24] Andersen TG, Bollerslev T, Diebold FX, Labys P. Modeling and forecasting realized volatility. Econometrica 2003;71(2):579–625. https://doi.org/10.1111/1468-0262.00418.
[25] Hill BM. A simple general approach to inference about the tail of a distribution. Ann Stat 1975;3(5):1163–74. https://doi.org/10.1214/aos/1176343247.
[26] Diebold FX, Mariano RS. Comparing predictive accuracy. J Bus Econ Stat 1995;13(3):253–63. https://doi.org/10.1080/07350015.1995.10524599.
[27] Christoffersen PF. Evaluating interval forecasts. Int Econ Rev 1998;39(4):841–62. https://doi.org/10.2307/2527341.
[28] Sensoy A. The inefficiency of Bitcoin revisited: a high-frequency analysis with alternative currencies. Financ Res Lett 2019;28:68–73. https://doi.org/10.1016/j.frl.2018.04.002.
[29] Zięba D, Kokoszczyński R, Śledziewska K. Shock transmission in the cryptocurrency market: is Bitcoin the most influential? Int Rev Financ Anal 2019;64:102–25. https://doi.org/10.1016/j.irfa.2019.04.009.
[30] Saengchote K. Decentralized lending and its users: insights from compound. J Int Finan Markets Inst Money 2023;87:101807. https://doi.org/10.1016/j.intfin.2023.101807.
[31] Franco JPM, Laurini MP. Quantifying systemic risk in cryptocurrency markets: a high-frequency approach. Int Rev Econ Finance 2025;102:104214. https://doi.org/10.1016/j.iref.2025.104214.